Int. J. Heat Mass Transfer. Vol. 10, pp. 1143–1158. Pergamon Press Ltd. 1967. Printed in Great Britain

THE HYPERSONIC VISCOUS SHOCK LAYER WITH MASS TRANSFER

S. Y. CHEN†, J. AROESTY† and R. MOBLEY‡
The RAND Corporation, Santa Monica, California

(*Received* 28 *June* 1966 *and in revised form* 15 *January* 1967)

Abstract—An investigation of the effects of surface mass transfer on the viscous hypersonic shock layer of a blunt body has been performed. Cheng's theory of the Newtonian shock layer has been modified to include both suction and injection, and extensive numerical results have been obtained for the injection of air into air.

These results indicate that the heat-transfer and skin-friction reductions due to injection can be adequately represented by the standard boundary-layer correlation formula for all but extreme low-density flows. As the Reynolds number decreases, however, mass transfer becomes ineffective in reducing heating rates and skin friction, especially for a very cold wall. The effect of nonzero wall temperature is to increase the shock-layer thickness dramatically, and there are also indications that the wall-temperature level determines whether the asymptotic inviscid-shock-layer thickness is approached from above or below.

NOMENCLATURE

B, mass ratio defined by equation (27a);
C_F, skin-friction coefficient defined by equation (29b);
C_H, heat-transfer coefficient defined by equation (29a);
C_p, specific heat at constant pressure;
f, nondimensional stream function defined by equation (24);
H, total specific enthalpy;
h, specific enthalpy;
K, Cheng's hypersonic viscous similarity parameter;
K_c, longitudinal curvature of the surface, $d\beta/dx$;
k, thermal conductivity;
M_∞, free-stream Mach number;
p, pressure;
$\bar{p}$, dimensionless pressure defined by equation (22);
Pr, Prandtl number, $C_p\mu/k$;
R, gas constant;
Re, Reynolds number;
Re_b, $\rho_\infty u_\infty R_N/\mu_0$;
R_N, nose radius;
s, distance along stream function, ψ;
T, temperature;
T_*, reference temperature, $=(T_w + T_0)/2$;
u, velocity component in x direction;
$\bar{u}$, dimensionless velocity defined by equation (22);
v, velocity component in y direction;
x, curvilinear coordinate;
y, coordinate normal to x axis;
Z, distance from the body surface to the axis of symmetry, $=R_N \cos\beta$.

Greek symbols

β, shock angle;
γ, ratio of specific heats;
Δ, shock standoff distance;
ϵ, $(\gamma - 1)/2\gamma$;
$\bar{\epsilon}$, density ratio, $\rho_\infty/\rho_o = (\gamma - 1)/(\gamma + 1)$;
η, Howarth-transform variable defined by equation (23);
θ, dimensionless total enthalpy ratio defined by equation (22);
θ', temperature-gradient parameter;

† Research Staff, Department of Geophysics and Astronomy.
‡ Research Staff, Computer Sciences Department.

μ, viscosity;
ν, zero for planar flow and unity for axisymmetric flow;
ξ, dimensionless coordinate defined by equation (23);
ρ, density;
φ, dimensionless tangential pressure gradient defined by equation (25);
ψ, stream function in von Mise's transformation defined by equations (15) and (16).

Subscripts

o, stagnation condition;
S, distance at shock;
w, condition at wall;
∞, free-stream condition;
$*$, reference condition;
1, condition in front of shock;
2, condition immediately behind shock (shock interface).

1. INTRODUCTION

HYPERSONIC viscous interactions on both slender and blunt bodies have been observed in low-density shock tunnels and wind tunnels during the past decade. These interactions, involving phenomena which are not contained within the usual framework of boundary-layer theory, have also been studied theoretically. There is a substantial body of analytical work available which modifies classical boundary-layer theory to include interaction effects [1, 2].

As interest develops in the possible application of lifting vehicles capable of operation at high lift-to-drag ratios at high altitudes, these problems of hypersonic viscous interaction move from the realm of academic interest to the realm of practical design considerations, which may be relevant to estimates of aerodynamic drag and heat transfer, as well as detailed flow-field structure.

The objective of this memorandum is to investigate the effects of surface mass transfer upon the viscous flow in the stagnation region of a vehicle in hypersonic flight at the upper edge of the continuum-flow regime. Stagnation enthalpy is high, but the lower density of the ambient air results in a thickening of the viscous layer, and interaction occurs between the boundary layer and the hypersonic shock layer. The usual concept of an outer inviscid flow determined by the body radius and the equilibrium shock conditions which provide the outer boundary conditions for a stagnation-point boundary-layer analysis is no longer valid. It becomes necessary to modify the Rankine-Hugoniot shock conditions to include the effects of viscous shear and heat conduction behind the shock. This modification requires a coupling between the boundary layer and the shock layer. Vorticity, which is generated by the shock layer, affects both shear stress and heat transfer, resulting, for example, in heating rates which are larger than those predicted by boundary-layer theory.

There are several different approaches to the study of hypersonic viscous stagnation flow, ranging from the complete higher-order boundary-layer theory of Van Dyke [3], Kao [4] and Maslen [5], which includes effects of vorticity interaction, slip, curvature and displacement thickness, to the integration of the Navier–Stokes equations performed by Levinsky and Yoshihara [6]. The approach which seems both tractable and relevant to the hypersonic cold-wall application is the viscous Newtonian thin-shock-layer theory. This theory, proposed by Cheng [7] and applied by him to a number of problems, has recently been given more formal treatment by Bush [8]. Bush has used the techniques of singular perturbation theory and matching asymptotic expansions to develop simplified equations, derived from the Navier–Stokes equations, involving six different layers, each with different variables. Cheng's theory, which essentially involves two layers, a thin shock-transition zone and a viscous Newtonian shock layer, is remarkable both for its simplicity and for its ability to yield the proper behavior for heat transfer in both the boundary-layer and

free-molecular limits. From the viewpoint of the designer, this is particularly useful, since it implies that it is not necessary to differentiate among the various flow regimes (boundary layer, vorticity interaction, transition, free molecule, etc.) in order to determine the appropriate theory for the calculation of heating rate. As long as the correct value of Cheng's similarity parameter is used, this single theory can be used to give a uniformly valid estimate of hypersonic heating rates at all altitudes.

The theory approximates the Navier–Stokes equations by boundary-layer equations which have been corrected for the centrifugal pressure gradient and which are valid between the body surface and the thin bow wave. The jump conditions across the shock wave are modified by the inclusion of viscous corrections. Hence, conditions behind the shock wave are not known until the entire flow field has been calculated.

This thin-layer approach permits the elliptic Navier–Stokes equations in the shock-layer region to be simulated approximately by a parabolic set of equations. The pressure-gradient terms are kept in both the normal and longitudinal momentum equations in order to insure the uniform validity of the theory at higher Reynolds numbers. The inclusion of the pressure-gradient term in the direction along the wall is important to the success of the theory in describing the vorticity interaction and boundary-layer regimes, where the pressure gradient along streamlines is small in the outer parts of the shock layer but important in the regions closest to the wall.

The present treatment of mass transfer into the hypersonic viscous shock layer is restricted to the injection of air into air and neglects all chemical effects by assuming that the equation of state is that of a single-component ideal gas. Certain higher-order effects, such as slip and temperature jump, are neglected. The viscosity–temperature law is assumed to be linear, through the use of a reference temperature based on the mean of the temperature behind the shock wave and the wall temperature. Cheng [9] has already demonstrated the accuracy of this last approximation in the context of viscous thin-shock-layer theory.

2. GOVERNING EQUATIONS AND BOUNDARY CONDITIONS

Cheng [7] has shown how the Navier–Stokes equations for flow past a blunt two-dimensional or axisymmetric body can be treated in two adjoining layers, a thin shock-transition zone and a viscous shock layer, if

$$\frac{1}{Re_b} + \bar{\epsilon} + \frac{1}{M_\infty^2} \ll 1$$

where Re_b is a modified free-stream Reynolds number, $\bar{\epsilon}$ is the density ratio, M_∞ is the free-stream Mach number, $1/Re_b$ is an estimate of the ratio of the shock thickness to body radius, and $(\bar{\epsilon} + 1/M_\infty^2)$ is an estimate to the ratio of shock-layer thickness to shock radius, Δ/R_S. If the layer is thin, then $\partial/\partial x \ll \partial/\partial y$, $y/R_N \ll 1$, and the following equations are valid for the description of the shock-transition zone (see Fig. 1):

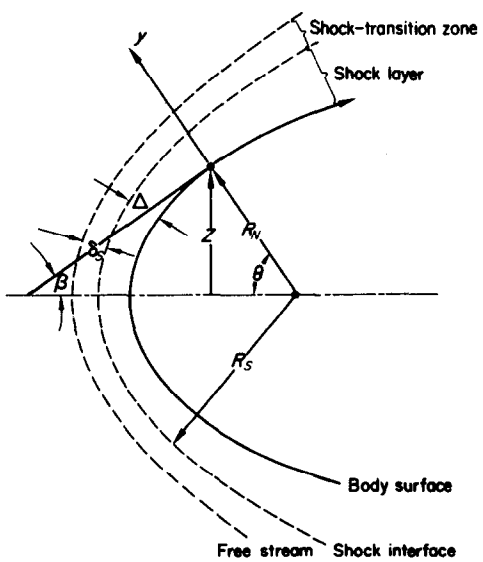

FIG. 1. Coordinate system for the shock and the body.

$$(\rho v)_y = 0, \tag{1}$$

$$\rho v u_y = (\mu u_y)_y, \tag{2}$$

$$p_y + \rho v v_y = \tfrac{4}{3}(\mu v_y)_y, \tag{3}$$

$$\rho v\left(h + \frac{u^2 + v^2}{2}\right)_y = \left[\mu\left(\frac{h}{Pr} + \frac{u^2}{2} + \frac{2}{3}v^2\right)_y\right]_y. \tag{4}$$

A gas with zero bulk viscosity has been assumed. The equations for the viscous shock layer, under the assumptions that $\partial/\partial x \ll \partial/\partial y$ and that there is strong shock compression, become

$$(\rho u Z^\nu)_x + (\rho v Z^\nu)_y = 0 \qquad \text{continuity} \tag{5}$$

$$p_x + \rho\left(u\frac{\partial}{\partial x} + v\frac{\partial}{\partial y}\right)u = (\mu u_y)_y \qquad \text{tangential momentum} \tag{6}$$

$$p_y + \rho K_c u^2 = 0 \qquad \text{normal momentum} \tag{7}$$

$$\left(\rho u\frac{\partial}{\partial x} + \rho v\frac{\partial}{\partial y}\right)H = \left\{\frac{\mu}{Pr}\left[H - (1 - Pr)\frac{u^2}{2}\right]_y\right\}_y \qquad \text{energy} \tag{8}$$

where

- H, total enthalpy $= C_p T + (u^2 + v^2)/2$;
- h, static enthalpy $= C_p T$;
- K_c, longitudinal curvature of the reference surface, $d\beta/dx$;
- Pr, Prandtl number;
- p, pressure;
- u, velocity component along the x axis;
- v, velocity component along the y axis;
- Z, distance between reference surface and the axis of symmetry;
- β, angle of incidence of the reference surface;
- μ, viscosity;
- ν, unity for axisymmetric flow and zero for planar flow;
- ρ, density;

and where $K_c u v \rho$ and other higher-order terms in v have been neglected. In addition, the ideal-gas law is assumed:

$$p = \rho R T. \tag{9}$$

The boundary conditions at the free stream are

$$\left.\begin{aligned} &\rho = \rho_\infty, && p = p_\infty, \\ &u = u_\infty \cos\beta, && h = h_\infty, \\ &v = -u_\infty \sin\beta. \end{aligned}\right\} \tag{10}$$

Integrating equations (1–4), introducing free-stream conditions from equation (10), and neglecting higher-order terms in v_2 yields

$$\rho_2 v_2 = -\rho_\infty u_\infty \sin\beta \tag{11}$$

$$-\rho_\infty u_\infty \sin\beta(u_2 - u_\infty \cos\beta) = (\mu u_y)_2 \tag{12}$$

$$p_2 = \rho_\infty u_\infty^2 \sin^2\beta \tag{13}$$

$$-\rho_\infty u_\infty \sin\beta(H_2 - H_\infty) = \left\{\frac{\mu}{Pr}\left[H - (1 - Pr)\frac{u^2}{2}\right]_y\right\}_2 \tag{14}$$

where the subscripts ∞ and 2 refer to the conditions at the free stream and shock interface, respectively.

Equations (11–14) are modified Rankine–Hugoniot conditions and indicate how the shock-jump conditions are modified by the effects of shear stress and heat conduction.

If the von Mises transformation is introduced,

$$\frac{\partial\psi}{\partial y} = \rho u(2\pi Z)^\nu \tag{15}$$

$$\frac{\partial\psi}{\partial x} = -\rho v(2\pi Z)^\nu \tag{16}$$

and x is replaced by s, then equation (5) is automatically satisfied and equations (6–8) can be reduced to

$$\frac{1}{\rho}\frac{\partial p}{\partial s} + u\frac{\partial u}{\partial s} = (2\pi Z)^{2\nu} u\left(\mu\rho u\frac{\partial u}{\partial\psi}\right)_\psi \tag{17}$$

$$\frac{\partial p}{\partial \psi} = -\frac{K_c u}{(2\pi Z)^\nu} \tag{18}$$

$$\frac{\partial H}{\partial s} = (2\pi Z)^{2\nu} \frac{\partial}{\partial \psi}\left\{\frac{\mu}{Pr}\rho u \times \left[H - (1 - Pr)\frac{u^2}{2}\right]_\psi\right\}. \tag{19}$$

These equations are those of a classical boundary-layer theory with the addition of a centrifugal pressure gradient across the shock layer. Mass transfer from the body surface is assumed to be in a purely radial direction, so that on the body surface the boundary conditions are

$$\left.\begin{aligned} u = 0 \qquad H = H_w \\ \rho v = \rho_{w_o} v_{w_o} \sin\beta \end{aligned}\right\} \tag{20}$$

at

$$\psi_w = -(\pi Z)^\nu \rho_{w_o} v_{w_o} Z.$$

Since $\sin\beta \approx 1$ in the stagnation region, this distribution of mass transfer corresponds to $\rho v = \rho_{w_o} v_{w_o}$ at the stagnation point.

In von Mises' variables, the modified shock conditions of equations (11–14) become

$$\left.\begin{aligned} \rho v &= -\rho_\infty u_\infty \sin\beta, \\ u &= u_\infty \cos\beta - (2\pi Z)^\nu \frac{\mu\rho u}{\rho_\infty u_\infty \sin\beta}\frac{\partial u}{\partial \psi}, \\ p &= \rho_\infty u_\infty^2 \sin^2\beta, \\ H &= H_\infty - (2\pi Z)^\nu \frac{\mu\rho u}{Pr\,\rho_\infty u_\infty \sin\beta}\frac{\partial}{\partial\psi} \times \left[H + (Pr - 1)\frac{u^2}{2}\right] \end{aligned}\right\} \tag{21}$$

and are the outer boundary conditions to the shock-layer equation, to be applied at $\psi_2 = (\pi Z)^\nu Z \rho_\infty u_\infty$.

Equations (17–19) subject to the boundary conditions of equations (20) and (21) are the set of equations governing the flow in the hypersonic viscous shock layer.

In order to perform a stagnation-line analysis, it is convenient to use the variables of boundary-layer theory, η and f.

First, dimensionless quantities are introduced

$$\left.\begin{aligned} \bar{p} = \frac{p}{\rho_\infty u_\infty^2 \sin^2\beta}, \qquad \bar{u} = \frac{u}{u_\infty \cos\beta} \\ \theta = \frac{H - H_w}{H_\infty - H_w}. \end{aligned}\right\} \tag{22}$$

In the stagnation region, $\beta \approx \pi/2$, and the pressure is independent of ψ, while the tangential pressure gradient is a function of both ψ and x. A tangential pressure gradient is included to insure that the flow at the base of the shock layer goes over to the correct flow at the edge of the boundary layer when the Reynolds number is large. The new independent variables are

$$\left.\begin{aligned} \xi &= \frac{S}{R_N} \\ \eta &= K(1 + \nu)^{\frac{1}{2}} \int_0^y \frac{\rho}{\rho_\infty}\frac{dy}{R_N} \end{aligned}\right\} \tag{23}$$

and the new dependent variable is

$$f(\eta) = \frac{K}{(1 + \nu)^{\frac{1}{2}}}\frac{\psi}{\rho_\infty u_\infty Z(\pi Z)^\nu}. \tag{24}$$

A linear-velocity law, $\mu = \mu_* T/T_*$, is assumed where μ_* is evaluated at T_*, a reference temperature. Equations (17) and (19) then reduce to

$$f''' + \frac{1}{1 + \nu} f'^2 + ff'' = -\frac{\epsilon}{1 + \nu}\left[\frac{H_w}{H_\infty} + \left(1 - \frac{H_w}{H_\infty}\right)\theta\right]\phi \tag{25}$$

$$\theta'' + Prf\theta' = 0 \tag{26}$$

where

$$\phi = 2\left[1 + \frac{1}{K(1 + \nu)^{\frac{1}{2}}}\int_\eta^{\eta_S} f'^2\, d\eta\right].$$

In boundary-layer theory, ϕ is a constant in the stagnation region. In the present theory, ϕ varies with the distance variable η and indicates the varying tangential pressure gradient due to the longitudinal curvature of the streamlines. If ϕ were constant, then equations (25) and (26) would correspond to the ordinary stagnation-point boundary-layer equations. With the inclusion of the varying tangential pressure gradient, equation (25) is somewhat more complicated than the corresponding boundary-layer equation.

The important new parameter involved in the solution is†

$$K^2 = \frac{\rho_\infty u_\infty R_N}{\mu_*} \epsilon \frac{T_*}{T_0}$$

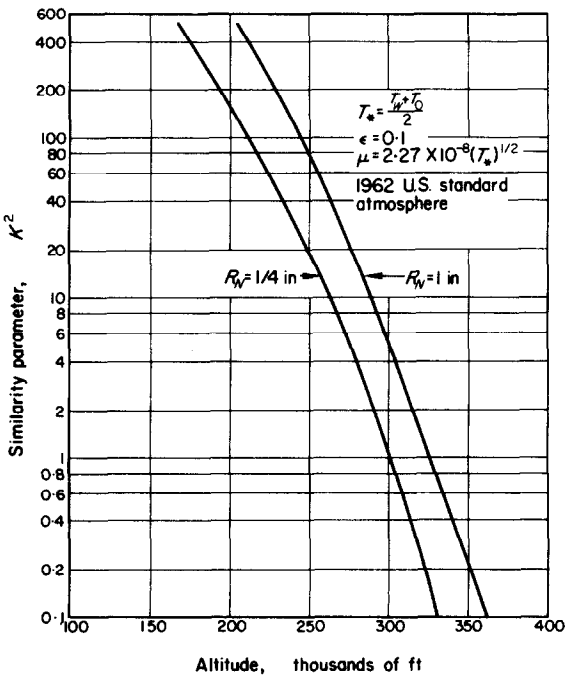

FIG. 2. Similarity parameter K^2 as a function of altitude (for all hypersonic velocities).

where T_0 refers to the stagnation temperature immediately behind the shock transition and is always less than the free-stream stagnation temperature because of the nonadiabatic shock transition, T_* is a reference temperature, and ϵ is defined as $(\gamma - 1)/2\gamma$. If T_* is taken as $(T_w + T_0)/2$ and μ_* is assumed to follow Sutherland's law at reference temperature T_*, then K^2 is a function only of altitude and nose radius for cold wall conditions. In other words, K^2 is not a function of velocity in the hypersonic flow regime, as shown in Fig. 2.

The associated boundary conditions at the body surface are

$$f(0) = -\frac{K}{(1+v)^{\frac{1}{2}}} \frac{\rho_{w_0} v_{w_0}}{\rho_\infty u_\infty}$$

$$\equiv \frac{K}{(1+v)^{\frac{1}{2}}} B \qquad \text{normal injection} \qquad (27a)$$

$$f'(0) = 0 \qquad \text{zero velocity slip} \qquad (27b)$$

$$\theta(0) = 0 \qquad \text{zero temperature jump.} \qquad (27c)$$

The boundary conditions at the shock location, where $\eta = \eta_s$, are

$$f(\eta_s) = \frac{K}{(1+v)^{\frac{1}{2}}} \qquad \text{mass flow} \qquad (28a)$$

$$f'(\eta_s) = 1 - \frac{(1+v)^{\frac{1}{2}}}{K} f''(\eta_s)$$

$$\text{viscous shear} \qquad (28b)$$

$$\theta(\eta_s) = 1 - \frac{(1+v)^{\frac{1}{2}}}{Pr\,K} \theta'(\eta_s)$$

$$\text{heat conduction.} \qquad (28c)$$

Equations (25) and (26) comprise a fifth-order system and require five boundary conditions. The additional boundary conditions of equations (27) and (28) are used to determine η_s, the location of the shock wave.

The heat-transfer coefficient C_H is defined as

$$C_H = \frac{-k_w(\partial T/\partial y)}{\rho_\infty u_\infty (H_\infty - H_w)}$$

or

$$C_H = \frac{(1+v)^{\frac{1}{2}}}{Pr} \frac{1}{K} (\theta')_{\eta=0} \qquad (29a)$$

† Cheng's hypersonic viscous similarity parameter (Fig. 2).

while the skin-friction coefficient

$$C_F = \frac{2}{\rho_\infty u_\infty^2}\left(\mu\frac{\partial u}{\partial y}\right)_w \tag{29b}$$

becomes

$$\frac{C_F}{\cos\beta} = 2(1+\nu)^{\frac{1}{2}}\frac{1}{K}f''(0). \tag{29c}$$

The shock standoff distance, Δ, can be expressed as

$$\frac{\Delta}{R_N} = \frac{\epsilon}{K}(1+\nu)^{-\frac{1}{2}}\left(1-\frac{H_w}{H_\infty}\right)\int_0^{\eta_S}\theta\,d\eta + \frac{\epsilon}{K}(1+\nu)^{-\frac{1}{2}}\frac{H_w}{H_\infty}\eta_S. \tag{29d}$$

3. DISCUSSION

The ordinary differential equations, equations (25) and (26), and boundary conditions, equations (27) and (28), were solved numerically on an IBM 7044 by employing the Adams–Moulton variable-interval integration technique and the Newton–Raphson convergence method (see Appendix).

The blowing rate B was varied from -1, corresponding to massive injection, to $+0{\cdot}3$, corresponding to suction. The case of suction was included in order to simulate the effect of leakage from the high-pressure air in the nose shock layer into the interior of the vehicle. This could occur if transpiration-cooling techniques were used and the coolant chamber pressure was not large enough to pump air into the shock layer, or if small gaps due to thermal expansion and deflection were formed in a nose shield.

The majority of the calculations were performed for an extremely cold wall, where $H_w/H_\infty \approx 0$. Several additional sets of calculations were performed using a moderately cold wall, $H_w/H_\infty \approx 0{\cdot}3$, in order to investigate the effects of nonzero wall temperature and to determine under what conditions the cold-wall results were a good approximation of finite wall temperatures.

The similarity parameter K^2 was varied from $0{\cdot}1$, corresponding to the extreme low-density regime, to 10^3, corresponding to the boundary-layer vorticity-interaction regime. No special precautions were taken in the calculation procedure to differentiate among these different regimes. The boundary-layer structure at large values of K^2 was calculated using the same techniques as those employed at low values of K^2, where no boundary layer is formed.

Temperature gradient $\theta'(0)$ and skin-friction parameter $f''(0)$

The nondimensional temperature gradient at the wall $\theta'(0)$ is shown in Fig. 3, while the skin-friction parameter $f''(0)$ is shown in Fig. 4. At low values of K^2, injection rates of the order of the free-stream mass flux ($B \sim -1$) are necessary to significantly decrease the heat transfer and skin friction from the zero-mass-transfer value. In the free-molecular limit ($K^2 \to 0$), mass injection has no effect on heat transfer from a cold wall ($H_w/H_\infty = 0$) if the energy accommodation coefficient is unity. It thus appears that this theory gives the correct limiting results for heat transfer to a very cold wall as the flow becomes free molecular, whether or not mass transfer is included. At high values of K^2, it seems clear that much smaller mass flow rates ($B \sim -0{\cdot}1$) are capable of reducing heat transfer and skin friction to values which are much lower than the zero-injection values. In particular, for the zero-temperature wall, a point of zero skin friction seems to be reached for fixed B and finite K^2. On the other hand, the few points that have been calculated here for the finite-temperature wall at a constant value of B ($B = -0{\cdot}1$) seem to indicate that the point of zero skin friction is reached asymptotically as $K^2 \to \infty$. This is true for the stagnation-point boundary layer if the wall temperature is nonzero. At large values of K^2 the flow structure should be well described by the usual theory for an inviscid shock layer and a viscous boundary layer.

Note that equation (25) in the neighbourhood of the wall ($\eta = 0$) becomes (if $H_w/H_\infty = 0$)

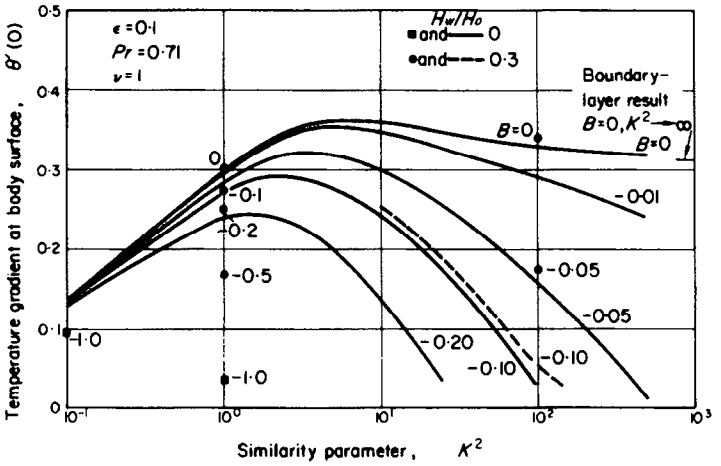

FIG. 3. Relation of temperature-gradient and similarity parameters (numbers on figure represent values of B).

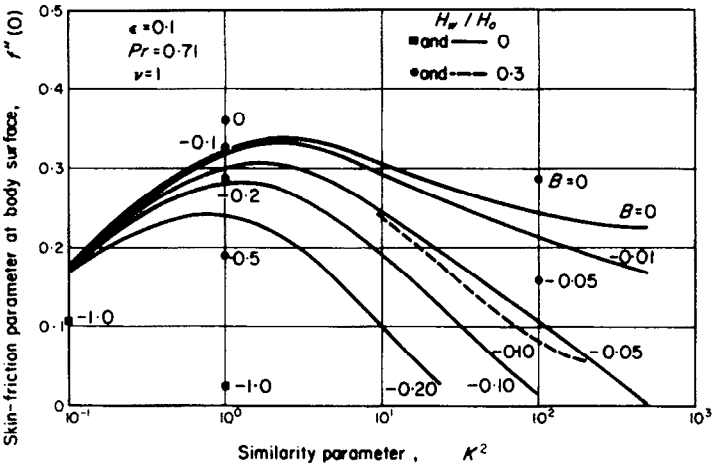

FIG. 4. Relation of skin-friction and similarity parameters (numbers on figure represent values of B).

$$f''' + ff'' = 0$$

the Blasius equation, subject to the injection boundary condition,

$$f(0) = +\frac{KB}{(1+\nu)^{\frac{1}{2}}}$$

and the no-slip condition becomes $f'(0) = 0$.

It is well known that solutions of the Blasius equation indicate a blowoff point (zero skin friction) at a finite value of $f(0) = -0{\cdot}876$, corresponding to $KB = -1{\cdot}23$ for zero skin friction. Extrapolation of present results to the point of zero skin friction $[f''(0) = 0]$ at a fixed value of the blowing rate implies that the skin friction is zero at $KB \approx -1{\cdot}15$, even at low values of K ($K^2 \approx 33$). There seems to be remarkably little effect of the wall-temperature ratio H_w/H_∞ on the temperature gradient while the skin-friction parameter increases with the

wall temperature. These results are known for ordinary stagnation-point boundary layers, and their extension to the hypersonic viscous shock layer is not unexpected.

Shock standoff distance

The shock standoff distance, Δ/R_N, is presented in Figs. 5 and 6. While the calculations were performed at sufficiently small values of K^2 such that fixed B and $K^2 \to \infty$ are not entirely relevant, a few comments about this limit are in order. If B is fixed and $K^2 \to \infty$, then the flow in the shock layer should be purely inviscid and consist of an outer layer of shocked gas and an inner layer of injectant, separated by a slip surface. Under these conditions, and particularly for $H_w/H_\infty < 1$, the injection layer is dominated by the tangential pressure gradient, while the outer layer is dominated by the centrifugal pressure gradient. The tangential velocity

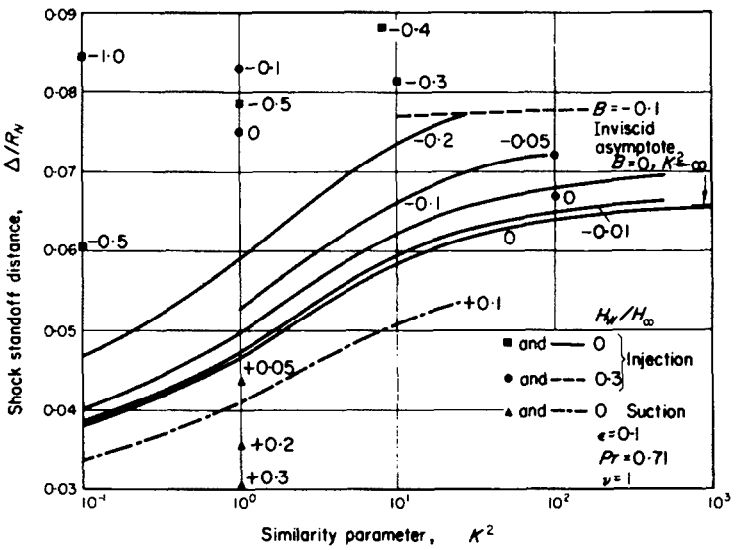

FIG. 5. Effects of mass injection or suction on shock standoff distance.

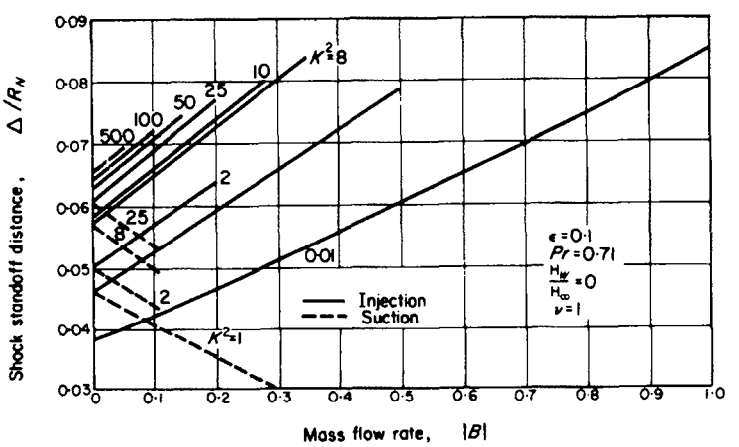

FIG. 6. Effects of similarity parameter on shock standoff distance.

ratio u/U_∞ in the inner layer is of the order $\sqrt{(H_w/H_\infty)}$, while the density ratio ρ/ρ_∞ in the inner layer is of the order H_∞/H_w. Consequently, the thickness of the injection zone is proportional to $1/\rho u$, or $\sqrt{(H_w/H_\infty)}$, and the asymptotic standoff distance should increase with increasing wall temperature from the zero-injection value. If H_w/H_∞ is zero, then these estimates indicate that the injection zone has zero thickness. The results shown in Figs. 5 and 6 have the following properties:

1. When the mass flow rate is fixed and the wall temperature is zero, the shock standoff distance increases with increasing K, seeming to approach an asymptotic limit. Similarly, if the density level (K) is fixed and the wall temperature is zero, then the shock standoff distance shows an almost linear variation with blowing rate.

2. The effects of nonzero wall temperature are most pronounced in the fully viscous regime [$K^2 \sim 0(1)$], where an increase of wall temperature from 0 to $H_w/H_\infty = 0{\cdot}3$ results in an increase in shock-layer thickness from 0·052 to 0·075. While the calculations for zero wall temperature show that the shock-layer thickness indicates an increase in Δ/R_N as K^2 is increased for fixed B, this is no longer true if a finite wall temperature is considered. For the case calculated ($H_w/H_\infty = 0{\cdot}3$), the standoff distance decreases with increasing K^2 and seems to be approaching an asymptote higher than the zero-temperature calculations. As $K^2 \to \infty$, this is to be anticipated in the light of the earlier discussion. For a fixed B ($B = 0{\cdot}1$), there is only a small decrease in Δ/R_N as K^2 increases from 1 to 100.

At a given altitude, velocity, and wall temperature, K^2 is a function of the blowing rate B, since the reference conditions employed in the temperature–viscosity relation are based on conditions behind the shock wave, which are affected by the injection. This point will be discussed again later.

Skin-friction and heat-transfer coefficients

In ordinary boundary-layer flows with mass transfer C_H/C_{H_0} and C_F/C_{F_0}, the heat-transfer ratio and skin-friction ratio based on reference conditions of zero mass transfer, are a function only of the blowing rate B multiplied by the square root of the appropriate Reynolds number. Since C_{F_0} and C_{H_0} are equal to constants multiplied by the square root of the same Reynolds number, then C_F/C_{F_0} and C_H/C_{H_0} are functions of B/C_{F_0} and B/C_{H_0}, respectively. An attempt has been made to use the same parameters in Figs. 7 and 8. However, in the hypersonic viscous thin-shock-layer theory, the dependence of C_{F_0} and C_{H_0} on K^2 is not known

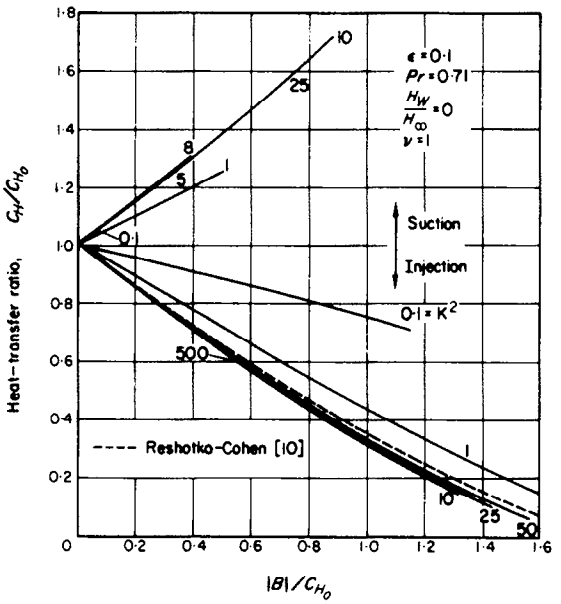

FIG. 7. Effects of mass injection or suction on heat-transfer coefficient.

explicitly, and consequently, Figs. 7 and 8 are presented as a convenient means of correlating all of the cold-wall calculations. The correlation becomes exact as K^2 increases and seems to go over to the results of Reshotko and Cohen [10]. In the low-density regime, $K^2 \approx 0{\cdot}1$, the correlation indicates the decreased effectiveness of mass transfer in reducing heat transfer, but for $K^2 > 1$, the correlation curves show that boundary-layer calculations, when presented in

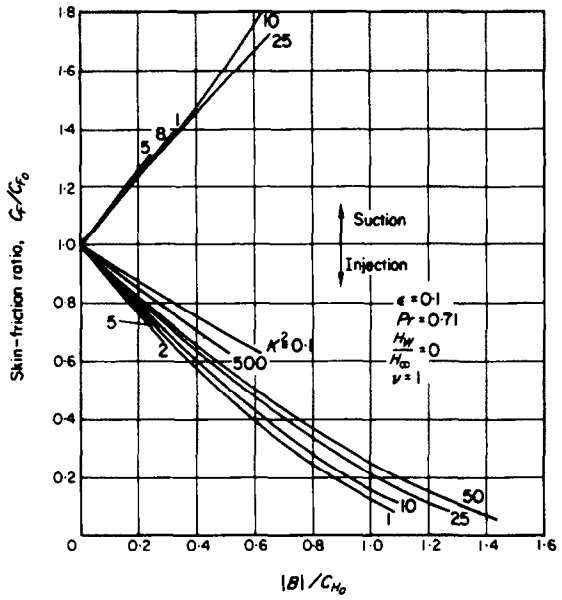

FIG. 8. Effects of mass injection or suction on skin-friction coefficient.

the form of Fig. 7, may be useful at much lower densities than might be anticipated.

Velocity and temperature distributions

The velocity ratio f' and the shear parameter f'' are shown in Fig. 9 for varying mass-flow ratios and different values of K^2, for the zero-temperature wall. The boundary-layer nature of the flow at large values of K^2 is clearly shown, while the fully viscous nature of the shock layer at low values of K^2 is also indicated. Mass transfer does not seem to change the postshock conditions very much, even at low values of K^2. This is also true of the temperature function θ, which is shown in Fig. 10. This lack of sensitivity of θ to mass transfer permits the use of a reference temperature T_*, which is based on the calculations for zero mass transfer. Consequently, at given free-stream conditions and nose radii, the parameter K^2, being only weakly dependent on the blowing rate, can be approximated by its zero blowing value.

At low values of K^2, injection rate comparable to the free-stream mass flow have a small effect on a shock layer which is completely viscous. The bow shock is pushed off, but the profiles exhibit no distinguished behavior. However, as the density is increased, and the more conventional boundary-layer–inviscid-layer profiles are obtained, dramatic changes in the profiles are caused by the injection. The shock wave

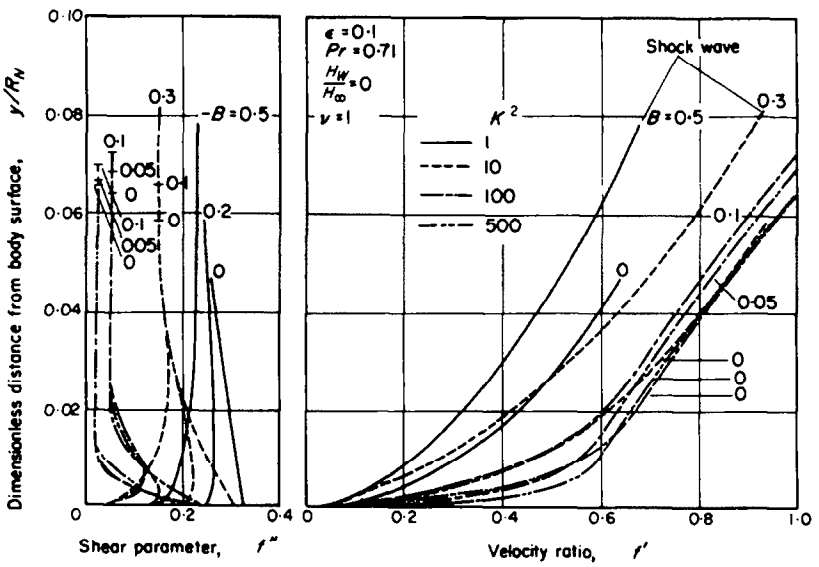

FIG. 9. Comparison of dimensionless velocity and shear-stress distributions (cold wall).

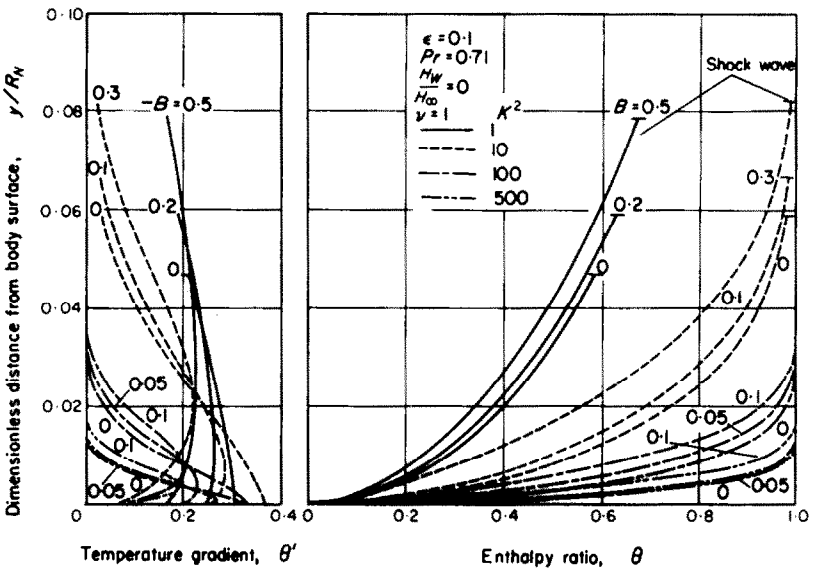

FIG. 10. Comparison of temperature parameter and heat-transfer distributions (cold wall).

does not seem to be pushed off very much by the injection, but there is clearly a large outer inviscid zone of small but constant shear and zero heat conduction, and then an intermediate thinner zone of large shear and heat conduction. The region closest to the wall seems to be included in this "shear layer", but the temperature gradient and shear at the wall are much lower than those in the center of the shear layer. However, there does not seem to be an appreciable regime near the wall where the heat conduction and shear stress are small; i.e. there does not seem to be an additional inviscid region near the wall. As noted earlier, the blowing rates employed were not sufficiently large to "blow off" the boundary layer.

The velocity, temperature, shear parameter, and conduction parameter θ' are shown in Figs. 11 and 12 for a nonzero wall temperature $(H_w/H_\infty) = 0.3$. At a fixed value of y, or at a fixed distance from the wall, θ for the zero-temperature wall is much greater than that for the finite-temperature wall. However, the temperature ratio $T/T_0 = H_w/H_\infty + (1 - H_w/H_\infty)\theta$ is not very different for both cases if K^2 and the mass-transfer rate are fixed; θ' at the wall seems to be almost independent of the wall temperature, but the distribution of θ' seems to be somewhat fuller with increased wall temperature.

In the lower-density regime, where $K^2 \sim 0(1)$, the effect of nonzero wall temperature is primarily to increase the extent of the shock layer. As in the case of zero heat transfer, the temperature at the shock wave seems to be only weakly affected by mass transfer. At large K^2, the finite temperature at the wall prevents the shear from decreasing significantly, since the pressure gradient acts to augment the skin friction in this case, while the infinite density at a zero-temperature wall renders the pressure-gradient effect negligible.

4. CONCLUSIONS

The theory developed by Cheng for the hypersonic viscous shock layer has been modified to include the effects of surface mass transfer. In addition, the theory for zero mass transfer has been applied to obtain numerical solutions for larger values of the similarity parameter K^2

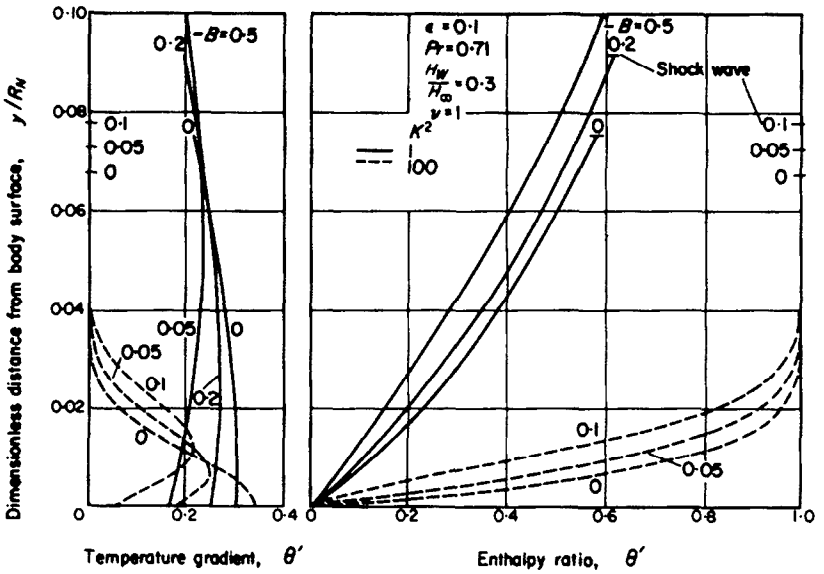

FIG. 11. Comparison of temperature parameter and heat-transfer distributions.

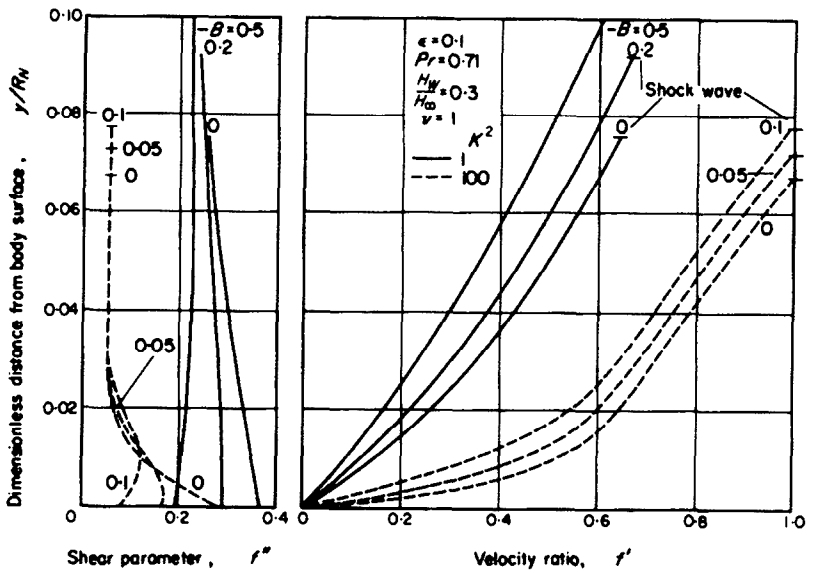

FIG. 12. Comparison of dimensionless velocity and shear-stress distributions.

than have been considered previously. Cheng's theory retains all the terms involved in the six-layer asymptotic expansion formulation of Bush, and through care and perseverance in computation, numerical results have been obtained for values of K^2 between 0·1 and 10^3.

The boundary-layer nature of the flow field at large values of K^2 contrasts with the fully viscous flow field at low values. The effects of mass transfer are to thicken the shock layer and decrease the heat transfer and skin friction. However, the results show that mass transfer is

ineffective in modifying the temperature and velocity profiles to reduce heat transfer and shear stress when $K^2 < 1$; for values greater than 1, the boundary-layer correlation formula, C_H/C_{H_o} = function of B/C_{H_o}, is useful for correlating the heating rate. Conditions behind the shock wave, which are considered as unknowns in this theory, are insensitive to mass transfer, so that the reference conditions involved in the computation of K^2 can be obtained from the results for zero mass transfer.

The effects of nonzero wall temperature are most pronounced for small values of K^2, where the shock-layer thickness is increased dramatically. There is a definite suggestion in these calculations that the increase of shock-layer thickness with increasing density ($K^2 \to \infty$) is only true for very cold walls. For walls that are not so cold, on the other hand, the shock layer seems to be thickest in the low-density limit ($K^2 < 1$) and approaches its asymptotic value for $K^2 \to \infty$ from above.

REFERENCES

1. C. F. DEWEY, Bluntness and viscous-interaction effects on slender bodies at hypersonic speeds, The RAND Corporation, RM-3832-PR (September 1964).
2. H. K. CHENG, Recent advances in hypersonic flow Research, *AIAA Jl* **1**(2), 295 (1963).
3. M. D. VAN DYKE, Second-order compressible boundary-layer theory with application to blunt bodies in hypersonic flow, SUDAER 112 or AFOSR TN 61-1270 (July 1961).
4. H. C. KAO, Hypersonic viscous flow near the stagnation streamline of a blunt body: II. Third-order boundary-layer theory and comparison with other methods, *AIAA Jl* **2**(11), 1898 (1964).
5. S. H. MASLEN, Second-order effects in laminar boundary layers, *AIAA Jl* **1**(1), 33 (1963).
6. E. S. LEVINSKY and H. YOSHIHARA, Rarefied hypersonic flow over a sphere, *Hypersonic Flow Research*, edited by F. R. RIDDELL, p. 81. Academic Press, New York (1962).
7. H. K. CHENG, Hypersonic shock-layer theory of the stagnation region at low Reynolds number, in *Proceedings 1961 Heat Transfer and Fluid Mechanics Institute*, p. 161. Stanford University Press, Stanford, Calif. (1961).
8. W. B. BUSH, On the viscous hypersonic blunt-body problem, *J. Fluid Mech.* **20**(3), 353 (1964).
9. H. K. CHENG and A. L. CHANG, Stagnation region in rarefied, high Mach number flow, *AIAA Jl* **1**(1), 231 (1963).
10. E. RESHOTKO and C. B. COHEN, Heat transfer at the forward stagnation point of blunt bodies, NACA TN 3513 (July 1955).

APPENDIX

Numerical Integration Technique

The computer program was written in FORTRAN IV for the IBM 7044. The numerical integration technique employed was fourth-order Adams–Moulton with a variable step size. Runge–Kutta is used to start the integration.

The convergence scheme used a modified Newton–Raphson type of iteration to converge to the boundary conditions at η_S. There are actually four boundary conditions, since φ must be reconstructed:

$$\varphi = 2\left(1 + \frac{1}{K(1+\nu)^{\frac{1}{2}}}\int_{\eta}^{\eta_S} f'^2\,d\eta\right)$$

$$= 2\left[1 + \frac{1}{K(1+\nu)^{\frac{1}{2}}}\left(\int_0^{\eta_S} f'^2\,d\eta - \int_0^{\eta} f'^2\,d\eta\right)\right].$$

Now if

$$Z = -\int_0^{\eta_S} f'^2\,d\eta + \int_0^{\eta} f'^2\,d\eta$$

then $Z' = f'^2$ may be written with the boundary condition $Z(\eta_s) = 0$. The state variables are then $f, f', f'', \theta, \theta', Z$. Boundary conditions at $\eta = 0$ are given for f, f', θ, but the values for f'', θ', Z which will satisfy the boundary conditions at η_S must be found. If one of the boundary conditions is chosen as a "stopping function" (Ω), there remain three boundary conditions $\{\psi_i\}$ which must be met. These were selected as follows:

$$\Omega = \frac{K}{(1+\nu)^{\frac{1}{2}}} - f = 0$$

$$\{\psi_i\} = \begin{Bmatrix} 1 - \dfrac{(1+\nu)^{\frac{1}{2}}}{K} f'' - f' \\ 1 - \dfrac{(1+\nu)^{\frac{1}{2}}}{Pr\,K}\theta' - \theta \\ Z \end{Bmatrix} = 0$$

and state variables $\{X_i\} = \begin{Bmatrix} f'' \\ \theta' \\ Z \end{Bmatrix}$ for convenience.

A set of initial trial values must be given for the $\{X_i\}_{\eta=0}$, then the differential equations integrated to the point where the stopping condition, $\Omega = 0$, is met. Usually the boundary values $\{\psi_i\} \neq 0$ the first time, and a new set of values for the $\{X_i\}_{\eta=0}$ must be found. This is done by computing a change in $\{X_i\}_{\eta=0}$ which will improve the initial estimates:

$$\{\Delta X_i\}_{\eta=0} = [F]^{-1}[W]\{\Delta\psi_i\}_{\Omega=0}.$$

The $[F]$ matrix is the matrix of partial derivatives of the boundary conditions at $\Omega = 0$ with respect to the state variables $\{X_i\}$ at $\eta = 0$:

$$[F] = \begin{bmatrix} \frac{\partial\psi_1}{\partial X_1} & \frac{\partial\psi_1}{\partial X_2} & \frac{\partial\psi_1}{\partial X_3} \\ \frac{\partial\psi_2}{\partial X_1} & \frac{\partial\psi_2}{\partial X_2} & \frac{\partial\psi_2}{\partial X_3} \\ \frac{\partial\psi_3}{\partial X_1} & \frac{\partial\psi_3}{\partial X_2} & \frac{\partial\psi_3}{\partial X_3} \end{bmatrix}.$$

These were found numerically by perturbing the $\{X_i\}$ one at a time.

The $[W]$ matrix is a weighting matrix which consists of only elements along the diagonal. Normally the unit matrix is used.

The $\{\Delta\psi_i\}_{\Omega=0}$ are the errors in the boundary conditions.

In conclusion, it must be pointed out that the convergence technique did occasionally "hang up", usually for the following reasons:

1. The numerical partial derivatives were not accurate. Solution: use smaller perturbations.
2. The changes in the $\{\psi_i\}$ became too nonlinear. Solution: reduce $[W]$.
3. The initial estimates for the $\{X_i\}_{\eta=0}$ were too far off. The expression "too far off" cannot be better defined, but it seemed to make much more difference what the initial trial values were when higher values of K^2 and B were used. Solution: run cases with small values of K^2 and B first and extrapolate to get a better estimate. (This was done off the machine.)
4. The integration became unstable. Solution: tighten the constants for error control in the integration routine.

It was sometimes difficult to distinguish between type 2 and type 4 difficulties, because type 4 could cause the nonlinearity of changes in the $\{\psi_i\}$.

Résumé— Une étude des effets du transport de masse superficiel sur la couche de choc hypersonique visqueuse d'un corps arrondi a été faite. La théorie de Cheng de la couche de choc Newtonienne a été modifiée pour inclure à la fois l'aspiration et l'injection, et l'on a obtenu de nombreux résultats numériques pour l'injection d'air dans l'air.

Ces résultats indiquent que les diminutions de transport de chaleur et de frottement pariétal dues à l'injection peuvent être représentées d'une façon adéquate par la formule standard de corrélation de la couche limite pour tous les écoulements à basse densité sauf les cas extrêmes. Cependant lorsque le nombre de Reynolds décroît, le transport de masse devient inefficace pour réduire le flux de chaleur et le frottement pariétal, spécialement pour une paroi très froide. L'effet d'une température pariétale non-nulle est d'augmenter considérablement l'épaisseur de la couche de choc; et il semble que la valeur de la température pariétale détermine si l'épaisseur de la couche de choc non visqueuse asymptotique est approchée par au-dessus ou par en-dessous.

Zusammenfassung—Für die zähe Hyperschallstossschicht wurden die Einflüsse des Stoffüberganges an der Oberfläche eines stumpfen Körpers untersucht. Die Theorie einer Newtonschen Stossschicht von Cheng wurde modifiziert, um sowohl Absaugung als auch Einblasung zu umfassen. Eine Vielzahl numerischer Ergebnisse wurde für die Einblasung von Luft in Luft erhalten.

Diese Ergebnisse zeigen, dass die Abnahme des Wärmeüberganges und der Oberflächenreibung infolge der Einblasung durch die üblichen Grenzschichtkorrelationsgleichungen für alle Fälle angemessen wiedergegeben werden können, mit Ausnahme von Strömungen bei extrem kleiner Dichte. Bei abnehmender Reynolds-Zahl verliert aber der Stofftransport seine Wirkung Aufheizung und Oberflächenreibung herabzusetzen. Das gilt besonders für sehr kalte Wände. Der Einfluss bei Wandtempraturen, die von null

verschieden sind, geht dahin die Stossschichtdicke stark zu erhöhen. Es liegen auch Anzeichen vor, dass die Grösse der Wandtemperatur bestimmend dafür ist, ob die Annäherung an die asymptotische nichtzähe Stossschichtdicke von oben oder von unten erfolgt.

Аннотация—Проведено исследование влияния конвективного поверхностного массообмена на гиперзвуковой ударный слой вязкой жидкости вблизи тупоносого тела. Модифицированная теория Ченга для ударного слоя ньютоновской жидкости учитывает отсос и вдув. Получено большое количество числовых данных для вдува воздуха в воздух.

Результаты показывают, что снижение коэффициентов теплообмена и поверхностоного трения, обсловленное вдувом, можно обобщить с помощью обычного уравнения пограничного слоя для всех течений за исключением жидкостей с очень низкой плотностью. Однако, при уменьшении числа Рейнольдса, массообмен не снижает скорости нагрева и коэффициента поверхностного трения, особенно для очень холодной стенки. Влияние стенки с температурой, отличной от нуля, заключается в чрезмерном увеличении толщины ударного слоя. Показано, что температурный режим стенки указывает на прближении к асимптотической толщине невязкого ударного слоя сверху или снизу.